THE ASTRONOMICAL JOURNAL, 121:2597–2609, 2001 May
© 2001. The American Astronomical Society. All rights reserved. Printed in U.S.A.

HUBBLE SPACE TELESCOPE-NICMOS OBSERVATIONS OF M31's METAL-RICH GLOBULAR CLUSTERS AND THEIR SURROUNDING FIELDS. II. RESULTS[1]

ANDREW W. STEPHENS AND JAY A. FROGEL
Department of Astronomy, Ohio State University, 140 West 18th Avenue, Columbus, OH 43210
WENDY FREEDMAN AND CARME GALLART
Observatories of the Carnegie Institution of Washington, 813 Santa Barbara Street, Pasadena, CA 91101
PASCALE JABLONKA
Observatoire de Paris, Place Jules Janssen, F-92915 Meudon Cedex, France
SERGIO ORTOLANI
Osservatorio Astrofisico di Asiago, Università di Padova, via dell'Osservatorio, I-36012 Asiago, Italy
ALVIO RENZINI
European Southern Observatory, Karl-Schwarzschild-Strasse 2, D-85748 Garching, Germany
R. MICHAEL RICH
Department of Physics and Astronomy, University of California at Los Angeles, Los Angeles, CA 90095
AND
ROGER DAVIES
Department of Physics, University of Durham, South Road, Durham DH1 3LE, England, UK
Received 2000 November 2; accepted 2001 January 22

ABSTRACT

We have obtained *HST*-NICMOS observations of five of M31's most metal-rich globular clusters: G1, G170, G174, G177, and G280. For the two clusters farthest from the nucleus, G1 and G280, we statistically subtract the field population and estimate metallicities using K-$(J-K)$ color-magnitude diagrams (CMDs). Based on the slopes of their infrared giant branches we estimate [Fe/H] $= -1.22 \pm 0.43$ for G1 and -0.15 ± 0.37 for G280. We combine our infrared observations of G1 with two epochs of optical *HST*-WFPC2 V-band data and identify at least one long-period variable (LPV) based on color and variability. The location of G1's giant branch in the K-$(V-K)$ CMD is very similar to that of M107, indicating a somewhat higher metallicity than our purely infrared CMD; [Fe/H] $= -0.9 \pm 0.2$. This latter value is more robust, and is supported by the presence of LPVs. For the field surrounding G280, we estimate the metallicity to be -0.3 from the slope of the giant branch, with a spread of $\sigma_{[Fe/H]} \sim 0.4$ based on the width of the giant branch. For the three central clusters, which are too compact for accurate cluster star measurements, we present integrated cluster magnitudes and CMDs for the surrounding fields. The K-band luminosity functions (LFs) of the upper few magnitudes of G1 and G280, as well as for the fields surrounding all of the clusters, are indistinguishable from the LF measured in the bulge of our Galaxy. This indicates that these clusters are very similar to Galactic globular clusters, and, at least in the surrounding fields observed, there are no significant populations of young luminous stars.

Key words: galaxies: individual (M31) — galaxies: star clusters

1. INTRODUCTION

Globular clusters (GCs) occupy a very special position in modern astrophysics. They provide the most stringent tests of stellar evolution theory, represent ideal templates for stellar population synthesis studies, allow age dating of galaxies with unrivaled precision, etc. The GC families of the Milky Way and its satellite galaxies, the Magellanic Clouds and the Fornax dSph galaxy, have been thoroughly studied from both the ground and space, especially with *HST*. The next nearest major GC family belongs to M31. To study individual stars in GC systems much more distant than M31 will require the next generation of ground or space based telescopes.

The GC systems of the the Milky Way and M31 appear to be quite similar in luminosity and color ranges (Battistini et al. 1987; Elson & Walterbos 1988; Huchra, Brodie & Kent 1991; Frogel, Persson, & Cohen 1980b; Frogel, Persson, & Cohen 1980c; Djorgovski et al. 1997; Seitzer, Banas, & Armandroff 1996). However, some of M31's bulge globulars appear to have line strengths as strong as those of giant ellipticals, suggesting metallicities considerably greater than any known Galactic globular (Bica et al. 1992; Jablonka, Alloin, & Bica 1992; Jablonka 1997). Burstein et al. (1984) has also noted that M31's GCs appear to follow different Hβ and CN correlations with Mg_2 with respect to Galactic globulars; they attributed this to the whole M31 GC family being systematically younger. Renzini (1986) pointed out that other interpretations were also possible, such as the chemical enrichment history of the two spheroids having proceeded with slightly different time scales, resulting in different element ratios.

HST observations of M31's GCs in the optical (with the goal of stellar photometry) started soon after the first refurbishing mission, with both FOC and WFPC2 (Fusi Pecci et al. 1996; Rich et al. 1996; Ajhar et al. 1996), and now

[1] Based on observations with the NASA/ESA *Hubble Space Telescope* obtained at the Space Telescope Science Institute, which is operated by the Association of Universities for Research in Astronomy (AURA), Inc., for NASA under contract NAS 5-26555.

include some of the most metal-rich clusters (Jablonka et al. 2000). The study of metal-rich M31 globulars complements similar studies of Galactic bulge globulars within this still poorly known, yet crucial part of age-metallicity space. Near-IR observations are essential to study the brightest giants in an old, metal-rich population, especially to determine bolometric luminosities. Metal-rich globular and bulge giants, which are the brightest bolometrically and in the near-IR, are in contrast, many magnitudes fainter at optical wavelengths because of severe molecular blanketing. In extreme cases, $(V-K)$ can be as great as ~ 10 at the top of the asymptotic giant branch (AGB; Frogel & Whitford 1987; Guarnieri et al. 1998), and these stars are likely to have escaped detection in M31 even with WFPC2.

In Cycle 7 we proposed to obtain NICMOS *JHK* images of five metal-rich globular clusters in M31. From these observations, we planned to achieve the following scientific goals: (1) explore the upper end of the GC luminosity function; (2) derive independent estimates for the metallicity of the M31 clusters and their adjacent fields from the slope and location of the near-IR RGB (Kuchinski et al. 1995); (3) determine the frequency of luminous RGB and AGB stars (including LPVs) per unit luminosity; (4) compare the cluster results with observations of M31 field stars (5) compare the properties of the luminous stars in M31's metal-rich clusters with those in the Galactic bulge and Galactic globulars; (6) integrate these results with optical photometry and spectroscopy and explore implications for stellar evolution theory and the interpretation of the integrated light of distant galaxies.

One critical issue deserves special attention if any of these goals are to be attained: the effect of stellar crowding. We have carefully analyzed the effects of blending on our NICMOS data (Stephens et al. 2001, hereafter Paper I). Through the creation of completely artificial clusters and fields, we have determined the proximity to each cluster where reliable photometry can be obtained. These simulations also allow us to quantify and correct for the effects of blending on the GB slope and width at different surface brightness levels.

This paper is organized as follows. Section 2 presents the reasons for selecting each cluster, and the details of the observations. Section 3 describes the reduction procedures, and gives a brief summary of the procedures and results on blending from Paper I. Section 4 presents the integrated photometry of the clusters, the CMDs and luminosity functions of the clusters and their surrounding fields, and metallicity estimates for G1, G280, and the G280 field. Our conclusions are summarized in § 5.

2. OBSERVATIONS

We have obtained *HST* NICMOS images of five of M31's metal-rich globular clusters and their surrounding fields (Cycle 7; Program ID 7826). These observations are summarized in Table 1. Column (1) lists the ID of Sargent et al. (1977), columns (2) and (3) give the coordinates of the center of each field observed with *HST*, and column (4) lists the angular separation of each field from the nucleus of M31. Columns (5)–(8) give previous metallicity estimates for each cluster based on: (5) absorption strengths from integrated optical spectra (Huchra et al. 1991); (6) spectroscopy of metal lines (Jablonka et al. 1992; Jablonka 1997); (7) RGB morphology (Fusi Pecci et al. 1996; Rich et al. 1996; Jablonka 1997); (8) integrated ground-based near-IR colors (Frogel et al. 1980b; Cohen & Matthews 1994). The last column (9) gives the observation date of each target.

G174 is the most metal-rich cluster known in M31 (Huchra et al. 1991; Jablonka 1997). It and G177 have spectra with line strengths comparable to those of strong lined ellipticals, and stronger than the most metal-rich Galactic globulars. G170's lines are somewhat weaker, but still comparable to those of two of the most metal-rich Galactic globulars, NGC6528 and NGC6553 (Barbuy et al. 1999; Cohen et al. 1999). G170, G174, and G177 are projected very close to the nucleus of M31. The G177 field, although not the closest to M31's nucleus, lies along the major axis of M31 and has the highest number of detected stars, ~ 7 arcsec^{-2} in our *K*-band images, as well as the highest background, $\mu_K \sim 15.4$ mag arcsec^{-2}.

G280's CMD has been characterized by Fusi Pecci et al. (1996) as similar to, but not quite as metal-rich, as NGC6553, consistent with its near-IR colors (Frogel et al. 1980b). In spite of G280's similarity to G170, it lies much farther from the nucleus of M31, at a distance of 20.5. G280 is also one of the most "open" clusters, making it one of the best clusters in our sample for individual stellar photometry.

Finally, G1 is the largest, brightest globular cluster in M31. This cluster is of particular interest because of its apparently high metallicity despite its large distance (152′; 35 kpc) from the center of M31. Since it nearly fills a NIC2 frame, we also observed a nearby field to estimate the background stellar contribution. It turns out that G1 is far enough from M31's center that field star contamination is

TABLE 1

M31 Globular Cluster Observations

				[Fe/H]				
ID[a] (1)	α (2000) (2)	δ (2000) (3)	r (arcmin) (4)	HBK (5)	JAB (6)	F-P (7)	NIR (8)	Date (UT) (9)
G001.....	00 32 47.2	39 34 48	152.3	−1.08	−0.52	−0.60 (?)	−1.38	1998.07.18
G170.....	00 42 32.4	41 10 29	6.1	−0.31	0.20	High	...	1998.08.10
G174.....	00 42 33.3	41 17 17	2.6	0.29	>0.5	...	−0.13	1998.08.13
G177.....	00 42 34.4	41 14 04	3.2	−0.15	0.52	High	−0.32	1998.09.08
G280.....	00 44 29.5	41 21 36	20.5	−0.70	...	−0.40 (?)	−0.40	1998.09.13

Note.—Units of right ascension are hours, minutes, and seconds, and units of declination are degrees, arcminutes, and arcseconds.

[a] Sargent et al. (1977).

TABLE 2
NICMOS FILTERS

FILTER	EXPOSURE (s)	FWHM (pixels)	FWHM (arsec)
F110W.....	1920	1.65	0.13
F160W.....	3328	1.95	0.15
F222M.....	2304	2.45	0.19

negligible, and our control field yielded only two stars over the entire 20″ dithered K-band field.

Our observations were taken with the NICMOS camera 2 (NIC2) which has a plate scale of $\sim 0\farcs0757$ pixel^{-1} and a field of view of 19.″4 on a side (376 arcsec^2). The NICMOS focus was set at the compromise position 1–2, which optimizes the focus for simultaneous observations with cameras 1 and 2. All of our observations used the MULTIACCUM mode (MacKenty et al. 1997) because of its optimization of the detector's dynamic range and cosmic-ray rejection. Parallel observations with NIC1 will be described in a later paper concentrating on M31's bulge.

Each of our targets was observed through three filters: F110W (0.8–1.4 μm), F160W (1.4–1.8 μm), and F222M (2.15–2.30 μm). These filters are close to the standard ground-based J, H, and K filters. The observation of each cluster spanned three orbits of *HST*, with ~ 42 minutes of observing per orbit. This yielded total integration times of 1920s in F110W, 3328s in F160W, and 2304s in F222M (see Table 2).

We implemented a spiral dither pattern with 4 positions to compensate for imperfections in the infrared array. The dither steps were 0.″4 for the J and K band images, and 5.″0 for the H band images. Thus the combined dithered images are $\sim 20''$ in J and K, and $\sim 24''$ in H. We used the predefined sample sequences STEP32 with 22 samples in J and 25 samples in K, and the STEP64 sequence with 21 samples in H.

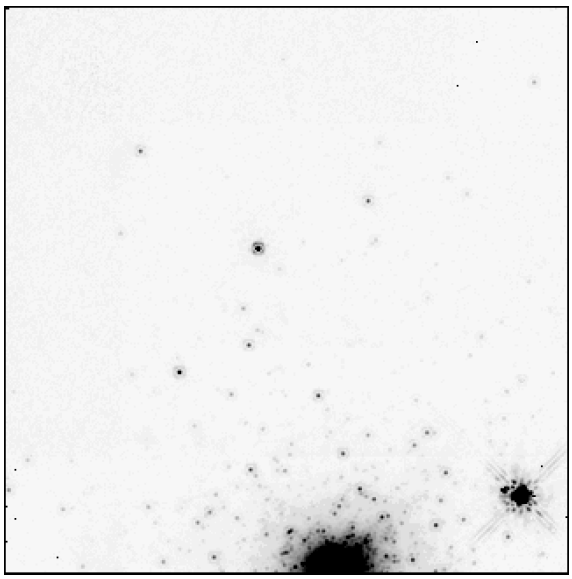


FIG. 1.—G1: F160W (H-band) combination of all four dithers; 3328 s total exposure. This image is $\sim 24''$ on a side. North is approximately up and east is approximately left because of the random rotation of the satellite. The faintest stars seen in this image have $H \sim 21.8$ mag. The object in the lower right corner is a foreground star and gives an idea of the full NICMOS PSF.

We present H-band images of each cluster in Figures 1 and 2. These images are the combination of four dither positions, and are $\sim 24''$ on a side. The H-band images are the deepest and also cover the most area as they were acquired using the largest dithers. Thus the H-band provides the deepest luminosity function, and gives us additional color information for LPV identification. The other analyses use primarily the J and K bands, as they are the bands where the groundbased comparisons and metallicity indicators exist.

3. DATA REDUCTION

Our data were reduced with the STScI pipeline supplemented by the Image Reduction and Analysis Facility (IRAF[2]) NICPROTO package (1999 May) to eliminate any residual bias (the "pedestal" effect). Object detection was performed on a combined image made up of all the dithers of all the bands (12 images in total). Point spread functions (PSFs) were determined from each of the four dithers, then averaged together to create a single PSF for each band of each target; the average full-width at half-maximum (FWHM) of each band is listed in Table 2. Instrumental magnitudes were measured using the ALLFRAME PSF fitting software package (Stetson 1994), which simultaneously fits PSFs to all stars on all dithers. DAOGROW (Stetson 1990) was used to determine the best magnitude in a 0.″5 radius aperture, which we then converted to the CIT/CTIO system using the transformation equations of Stephens et al. (2000).

The azimuthally averaged number of detected stars per square arcsecond for each cluster is shown in Figure 3 as a function of radius from the cluster center. The counts include stars which were measured at least once in any band. Even though it appears we have detected stars into the centers of all the clusters, we have demonstrated in Paper I that the detections near the cluster cores are spurious, the result of image blending. The three clusters near the center of M31, G170, G174, and G177, have central spikes in the number counts, but quickly fade into the background. No photometry is possible for individual stars in these clusters. For the two less compact clusters, G1 and G280, the number of detections decreases gradually with radius, and stellar photometry is possible in their outer regions.

3.1. *Blending Analysis*

Stellar photometry in crowded regions such as we have observed can be strongly affected by blending. In order to quantify and attempt to correct for the effects of blending, we have performed several types of artificial star experiments. Paper I describes in detail experiments where we constructed completely artificial clusters. Starting with a blank frame having the appropriate noise characteristics, we added stars according to the cluster's radial profile. The input stellar population was chosen to match the luminosity function and colors of giants observed in the Galactic bulge. The artificial frames were then processed and measured in

[2] IRAF is distributed by the National Optical Astronomy Observatories, which are operated by AURA, under cooperative agreement with the National Science Foundation.

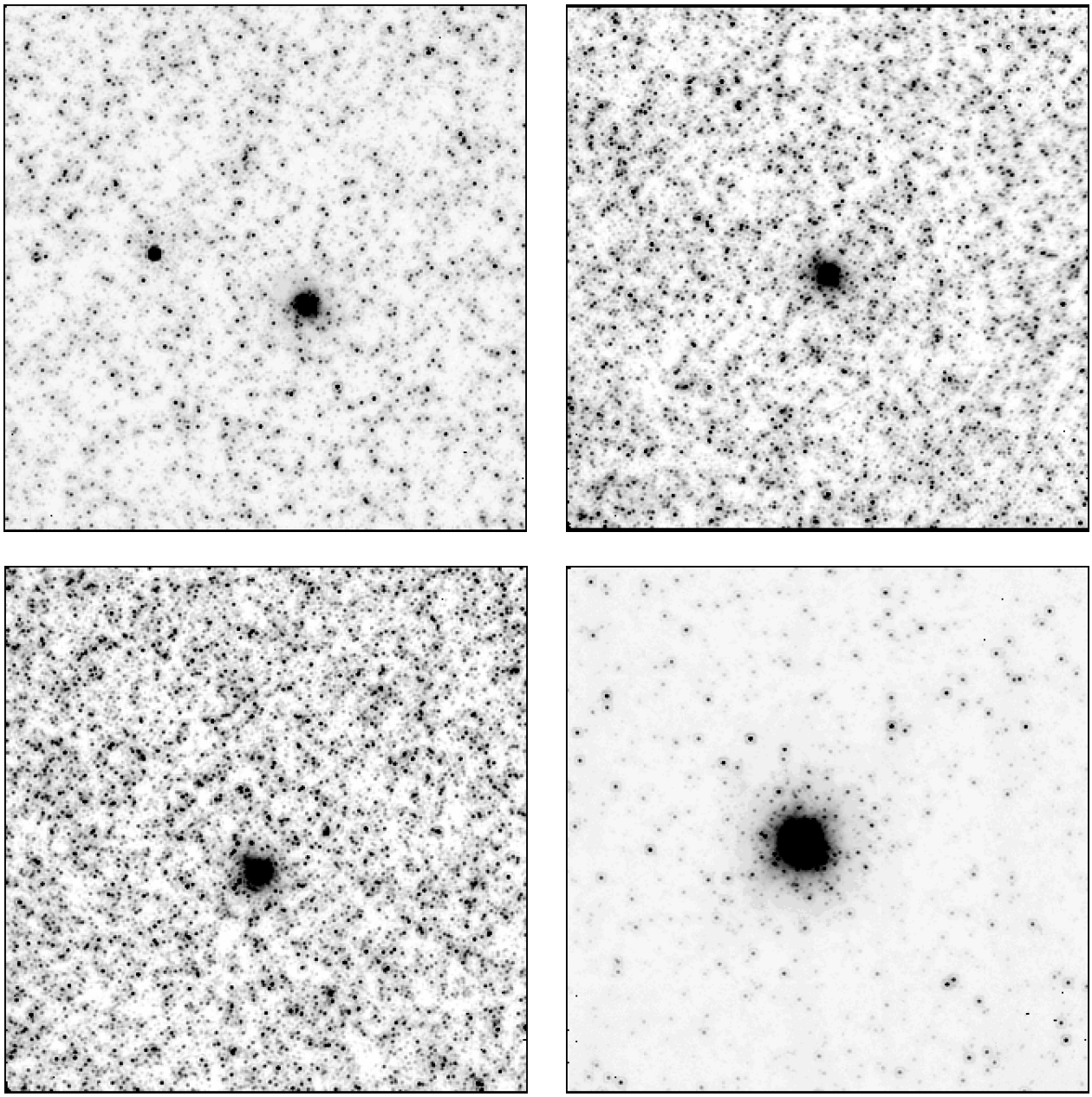


FIG. 2.—Combination of four dithers in the F160W (*H*) filter, yielding 3328 s total exposure time. Each image is ~24″ on a side, and all images are windowed identically. North is approximately up and east is approximately left because of variations in the orientation of the satellite for each image. *Top left*: G170; *top right*: G174; *bottom left*: G177; *bottom right*: G280.

exactly the same manner as the real data. The CMDs and LFs from the artificial clusters can be used to determine the origin of objects seen in the real CMD, and to assess the validity of our measured LFs.

To better study the effects of blending at different surface brightness levels, we have also created uniformly populated mini-fields. Constructed in the same manner as the artificial clusters, these 100 × 100 pixel fields each have between 10^4 and $\sim 5 \times 10^6$ stars, enough to reach the surface brightnesses observed in the cores of these M31 clusters.

Using Figure 9 of Paper I, which shows the difference between the recovered and input stellar magnitudes as a function of the field surface brightness, we have chosen $\mu_K = 16$ mag arcsec^{-2} as the threshold surface brightness where our photometry starts to become noticeably affected by blending, and $\mu_K = 14$ mag arcsec^{-2} as the critical surface brightness where our photometry is dominated by blends and no longer yields any useful information. Brighter than this level, no measurements are reliable. If one desires to accurately measure stars fainter than those we have measured, the threshold surface brightness will have to be fainter than $\mu_K = 16$.

Figure 4 shows azimuthally averaged *K*-band surface brightness profiles of each cluster. We use this plot to determine the threshold-blending radius (R_{16}; where $\mu_K = 16$ mag arcsec^2), and the critical-blending radius (R_{14}; where $\mu_K = 14$ mag arcsec^2) of each cluster. These levels are indicated by the dotted lines in Figure 4, and the resulting radii are are listed in Table 3. Any objects measured inside the threshold-blending radius, especially faint objects, are

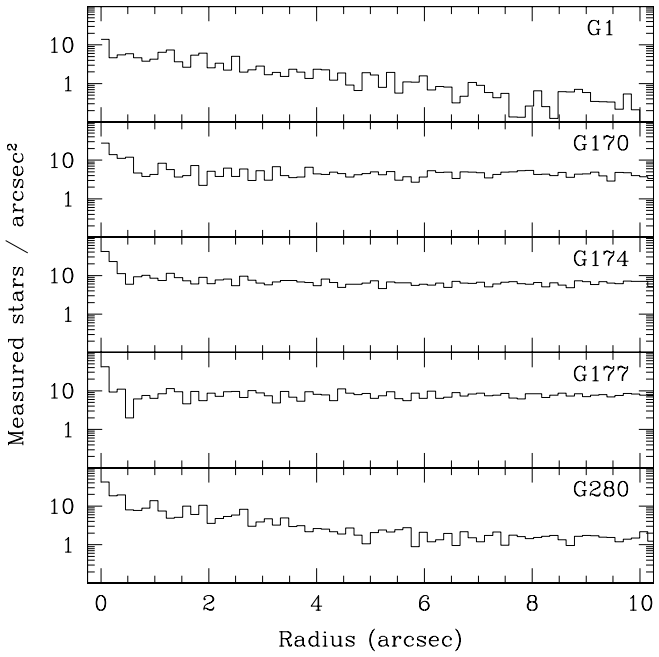


FIG. 3.—Azimuthally averaged number counts as a function of radius from the cluster center. Note the difference between the sharp peak in counts seen in the three compact central clusters (G170, G174, and G177) and the gradual decline in counts of the two more distant clusters (G1 and G280).

potentially affected by blending, and should be considered suspect. (Note that the radius R_{16} was chosen so that stars input at $M_K \sim -3$ could be recovered accurately most of the time. However, for stars fainter than this, there is no way to tell whether they are blends or not.) Objects measured inside the critical-blending radius are undoubtedly blends,

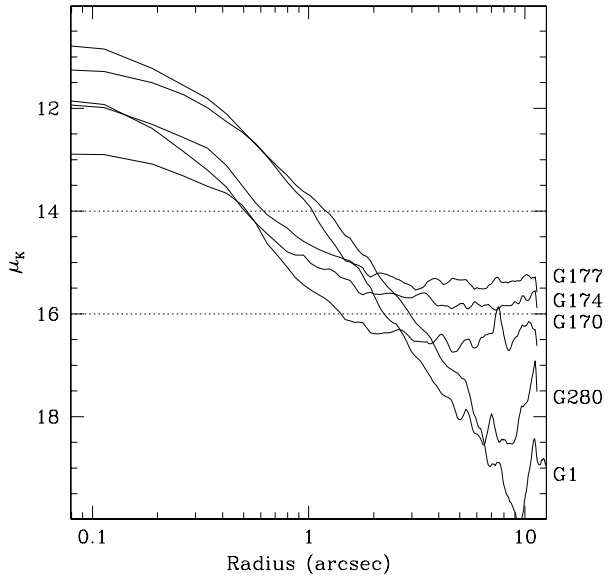


FIG. 4.—Azimuthally averaged K-band surface brightness (magnitudes per square arcsecond) as a function of radius from the cluster centers. The dotted lines show the chosen critical blending surface brightness ($\mu_K = 14$) and threshold blending surface brightness ($\mu_K = 16$). The intersections of these lines with the cluster profiles determines the critical and threshold radii for each cluster. Note that the G174 and G177 profiles never drop below the threshold blending limit of $\mu_K = 16$.

TABLE 3

THRESHOLD AND CRITICAL BLEND RADII

Cluster	Core μ_K	R_{14}	R_{16}
G001.....	11.2	1.2	2.9
G170.....	12.9	0.5	1.4
G174.....	11.7	0.5	...
G177.....	11.8	0.6	...
G280.....	10.7	1.0	2.2

and although we plot them for completeness, they should be disregarded.

Since we want to use the slope of the GB $[\Delta(J-K)/\Delta(K)]$ to estimate metallicities (Kuchinski & Frogel 1995), and the width of the GB to place limits on any spread in metallicity, we have investigated the effects of crowding on these quantities. At low surface brightnesses ($\mu_K \sim 20$ mag arcsec^{-2}) blending has a negligible effect on the measurement of the GB slope, and the correct metallicity is calculated. As the surface brightness increases to $\mu_K \sim 13$ mag arcsec^{-2}, the recovered GB slope also increases (becomes more negative), yielding an artificially greater metallicity. Plotting the recovered GB slope as a function of surface brightness from the artificial frames, we have determined a linear correction to the slope in an attempt to account for the effects of blending (Fig. 11, Paper I); we apply this relation to our observed slope to improve our metallicity determinations. The true change in slope due to blending will, of course, depend upon the true luminosity function and colors of the stellar population.

4. PHOTOMETRY

Here we present the integrated cluster photometry and individual stellar photometry for the clusters and fields. Using the criteria developed in Paper I, and summarized in § 3.1 here, we reject measurements which may be affected by blending. As stated above, cluster star measurements could only be extracted for the two less compact clusters G1 and G280. For these two clusters we perform statistical subtraction of the field to yield a cluster GB. Our simple technique to do statistical subtraction spatially divides the frame into cluster or field, then partitions each group into bins 1 mag wide in J and K; we chose rather wide bins to allow for spread due to blending. The number of field stars per bin is then normalized by multiplying by the ratio of the cluster to field areas, and the appropriate number of suspected field stars are randomly subtracted from each of the cluster star bins. We perform an iterative linear least-squares fit to the GB using stars brighter than $M_K = -3.7$ and $M_J = -2$ and throwing away 3 σ outliers. We then estimate the cluster metallicity using the GB slope technique (Kuchinski et al. 1995; Kuchinski & Frogel 1995), and compare the M31 GBs with those measured for Galactic clusters. For the three central clusters, we present only the surrounding field photometry in § 4.5.1. The data are presented in the form of M_K-$(J-K)$ diagrams, as well as luminosity functions, and a V-$(V-K)$ diagram of G1 using optical WFPC2 data.

In this paper we assume a distance modulus to M31 of $(m-M)_0 = 24.4$, and unless specified otherwise, we do not correct for extinction or reddening. For reference, Frogel et al. (1980b) has measured $E(V-K) = 0.28$ for G1 and G280, which corresponds to $E(J-K) = 0.06$ and $A_K = 0.03$. More recently Barmby et al. (2000) have determined reddenings

for a large sample of M31 clusters. The distribution of 221 reliable reddening measurements has a mean of $E(B-V) = 0.22$ with a standard deviation of 0.19. This average value corresponds to $E(J-K) = 0.12$ and $A_K = 0.07$. Although metallicity determinations based on the slope of the GB are insensitive to reddening, differential reddening across a field could mimic a spread in metallicity. This will be discussed in § 4.5.3.

4.1. *Integrated Photometry*

We have used simple aperture photometry to measure the integrated magnitudes of the G170, G174, G177, and G280 clusters. These measurements are listed in Table 4. The three central clusters (G170, G174, and G177) are very compact, and an aperture of 40 pixel (3.″03) radius is chosen as the optimum compromise between the maximum aperture size and best sky measurement. G280 is more extended, and we therefore use a larger 60 pixel (4.″54) radius aperture. The sky was measured as the average of an annulus around the clusters, using the largest outer radius possible, typically 60 pixels wide, stopping just short of the high background region at the bottom of all of the K-band frames.

Since we are resolving the background stars, the sky estimate is sensitive to the size and location of the background region. To estimate the errors of this sky averaging, we have divided each cluster's original single large sky annulus into three smaller annuli. We use the dispersion in the measured cluster magnitudes and colors from these four different annuli to quantify the errors. We find that the formal IRAF errors seem to reflect the dispersion in measurements very well; however we use the larger of these two estimates as our quoted K-band errors. Since the errors in each band are correlated, the errors in colors tend to be much smaller. Using the dispersion in measured colors from the four annuli, we estimate the error in both colors $(J-K)$ and $(H-K)$ is 0.01 mag.

Previous measurements are listed on the right side of Table 4. Frogel et al. (1980b) used single-channel photometry with a 7.″5 radius aperture. The Cohen & Matthews (1994) and Barmby et al. (2000) works used infrared arrays with 2.″8 and 6″ radius apertures, respectively. Because of the limited size of our array we were unable to match the large apertures of some of the previous measurements. However, our excellent resolution allows us to very carefully place our measurement aperture and sky annulus (e.g., to avoid the bright field star ~7.″4 from G170). The good color agreement but poor magnitude agreement with previous observations suggests a measurement problem that is present in all bands and thus cancels out in the color determination. The most likely cause is the difference in the cluster and sky measurement regions between us and previous authors.

4.2. *G1*

The M_K-$(J-K)$ color magnitude diagram for the G1 cluster is shown in Figure 5. The left panel shows all the cluster data from the G1 frame. Open circles indicate objects which are located inside the threshold-blending radius (2.″9) or lie in a region of high background in the lower 25 pixels of the the K-band frames (on the CMD, these stars include all objects with $(J-K) > 1.6$ and a similar number of objects bluer and fainter). Objects inside the critical-blending radius (1.″2) are plotted with half-size dots. The center panel shows the (two) objects measured in the adjacent control field located 64″ southeast of G1. The right panel shows only good measurements of cluster stars. Potentially blended objects and objects within 25 pixels of the bottom of the frame have been removed, and (two) field stars have been statistically subtracted.

We applied a linear least-squares fit to the cluster stars on the upper GB, only using stars brighter than $M_K = -3.7$ and $M_J = -2$, the 50% completeness limits, and ignoring 3 σ outliers. The best-fit equation is displayed at the top of the right panel. We then used the relationship between the GB slope $[\Delta(J-K)/\Delta(K)]$ and globular cluster metallicity derived by Kuchinski et al. (1995) and Kuchinski & Frogel (1995) for Galactic globulars to estimate the cluster metallicity. This relation states that $[\mathrm{Fe/H}] = -2.98\text{–}23.84 \times \mathrm{slope}_{\mathrm{GB}}$. Our measured GB slope is -0.083 ± 0.014, which implies a blending-uncorrected metallicity of -1.00 ± 0.42. The error estimate is a quadratic combination of the error in our linear fit, and the quoted 0.25 dex scatter observed in the GB slope-metallicity relation. We note however, that the range in our fitted luminosity ($\Delta M_K \sim 2.5$ mag) is only barely larger than half of the range used to define the relation ($\Delta M_K \sim 4.5$ mag) Kuchinski & Frogel (1995), slightly decreasing the confidence of our estimate.

As discussed in § 3.1, the measured slope of the GB is affected by blending, and the magnitude of the distortion is a function of surface brightness. Ideally we would calculate the GB slope in several annuli around the cluster and correct each according to the surface brightness of that annulus. In reality, there are so few stars measured on the upper GB to begin with that splitting it up into even two annuli degrades the accuracy of the slope determination significantly. Thus we take a number-weighted average surface brightness of $\mu_K = 18.4$ mag arcsec^{-2} for all usable

TABLE 4

INTEGRATED PHOTOMETRY

	NICMOS				GROUND-BASED			
CLUSTER	K	$J-K$[a]	$H-K$[a]	ap	K	$J-K$	$H-K$	ap
G170	12.93 ± 0.05	0.99	0.37	3.0	12.84	0.98	...	6.0[b]
G174	12.56 ± 0.04	1.03	0.47	3.0	12.84	1.00	...	2.8[c]
G177	12.36 ± 0.04	0.98	0.39	3.0	12.50	0.92	...	2.8[c]
G280	10.91 ± 0.02	0.90	0.34	4.5	11.06	0.88	0.15	7.5[d]

[a] The error in $(J-K)$ and $(H-K)$ is 0.01 mag.
[b] Barmby et al. (2000).
[c] Cohen & Matthews (1994).
[d] Frogel et al. (1980b).

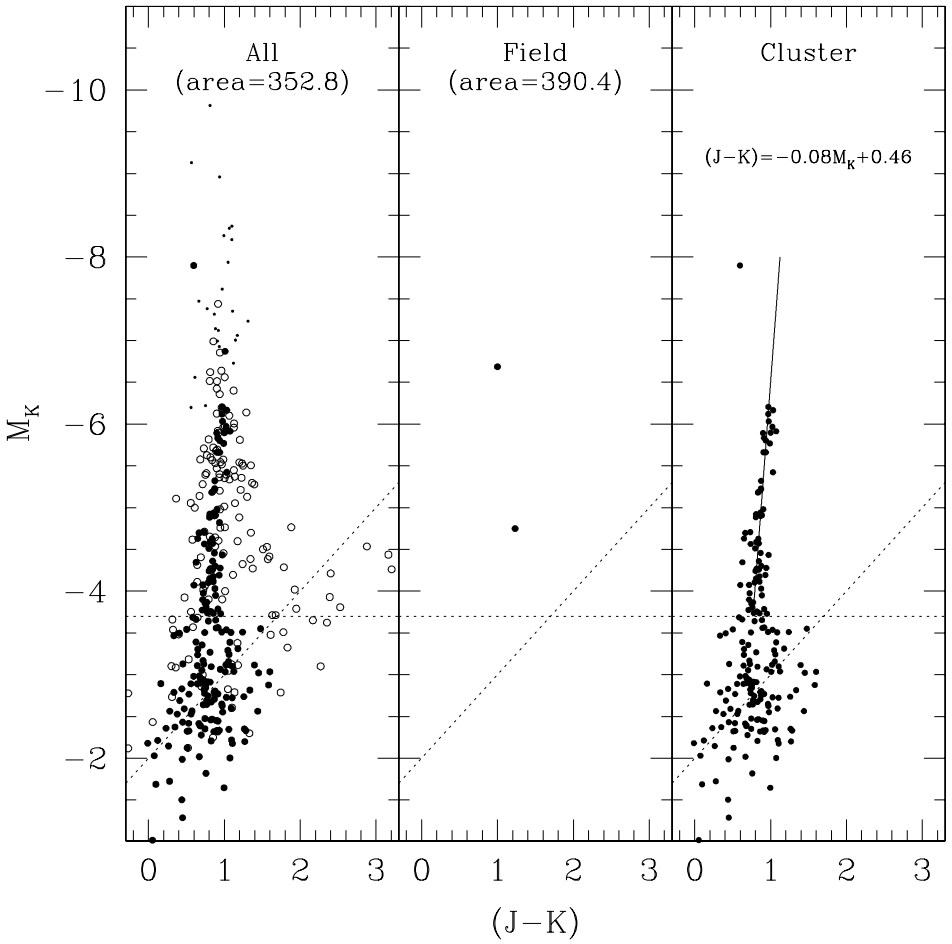


FIG. 5.—*Left*: All 355 objects measured on the G1 frame. Open circles indicate objects within the threshold-blending limit ($\mu_K < 16, r < 2\farcs9$) or within 25 pixels of the bottom of the *K*-band image. Half-size dots are for objects inside the critical-blending limit ($\mu_K < 14, r < 1\farcs2$). *Center*: The two stars measured in the adjacent control field 64″ southeast of G1. *Right*: The 191 remaining cluster stars after potential blends, noisy measurements, and field stars have been removed. The linear fit to the GB above the 50% completeness limits of $M_K = -3.7$ and $M_J = -2$ (*dashed lines*) is shown at the top.

cluster photometry, which leads to a metallicity correction of -0.22 ± 0.09 dex, where the error of 0.09 dex is the rms scatter around our correction. This gives a final metallicity estimate of -1.22 ± 0.43 for G1.

We have combined our infrared NICMOS data with the *V*-band WFPC2 observations of Rich et al. (1996) from 1994 July 29 and Meylan et al. (2001) from 1995 October. The resulting M_{K_0}-$(V-K)_0$ CMD is shown in Figure 6. In this diagram, the points indicate the mean $(V-K)_0$ obtained from both optical data sets. The errorbars illustrate the range of the observed *V*-band measurements. Since the measurement errors are relatively small, any large deviations are assumed to be indicative of stellar variability. Thus several of the most luminous stars near the top of the GB are undoubtedly variables. We have also overplotted the RGB ridge lines of M13 and 47 Tucanae from Frogel, Persson, & Cohen (1981) and stars in M107 measured by Frogel, Persson, & Cohen (1983). The G1 RGB position and morphology in this CMD indicates that G1 probably has a slightly higher metallicity ([Fe/H] ~ -0.9) than we obtained from the slope of the infrared GB.

Previous measurements of G1's metallicity are listed in Table 5. Harris & Canterna (1977) used Washington photometry of the integrated light to obtain a value of -0.3. Frogel et al. (1980b) used the integrated $(V-K)$ colors and the infrared CO index, finding [Fe/H] $= -1.22$. Bònoli et al. (1987) recalibrated the Frogel results using the new [Fe/H] values of Zinn & West (1984), obtaining [Fe/H] $= -1.23$. Based on the GB position in the I-$(V-I)$ CMD, Heasley et al. (1988) estimated a metallicity of about -0.7, and Rich et al. (1996) found a metallicity "at least as high as 47 Tuc." Using the strengths of absorption features in integrated optical spectra, Huchra et al. (1991) found a metallicity of -1.08. Averaging the metallicities from many metallic lines in the spectral range 3200–9750 Å, Jablonka et al. (1992) determined $\log(Z/Z_0) = -0.52$. Using the

TABLE 5

G1 AND G280 METALLICITIES

Reference	G1	G280
Harris & Canterna (1977)	−0.3	0.0
Frogel et al. (1980b)	−1.22	−0.19
Bònoli et al. (1987)	−1.23	−0.37
Heasley et al. (1988)	−0.7	...
Huchra et al. (1991)	−1.08	−0.70
Jablonka et al. (1992)	−0.52	...
Rich et al. (1996)	−0.8	...
Fusi Pecci et al. (1996)	−1.14	−0.44
Meylan et al. (2001)	-0.95 ± 0.09	...
This work: $(J-K)$ CMD	-1.22 ± 0.43	-0.15 ± 0.37
This work: $(V-K)$ CMD	-0.9 ± 0.2	...

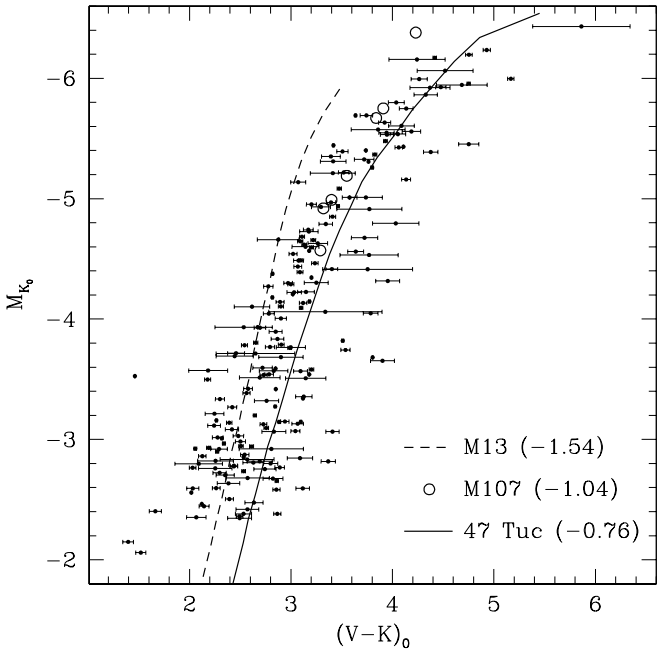


FIG. 6.—G1 CMD created through the combination of our K-band data with the WFPC2 V-band observations of Rich et al. (1996) and Meylan et al. (2001). The points are the mean $(V-K)_0$ from both optical data sets, and the error bars illustrate the difference between the two optical data sets. Thus large error bars indicate variability at the top of the CMD and most likely misidentifications at the bottom of the CMD. G1 has been corrected for distance and reddening with $(m-M)_0 = 24.4$, $A_K = 0.03$, and $E(V-K) = 0.28$ (Frogel et al. 1980b). Overplotted are the giant branch ridge lines of M13 (*dashed line*) and 47 Tuc (*solid line*) from Frogel et al. (1981). Measurements of single stars in M107 from Frogel et al. (1983) have also been plotted for reference. The metallicities (*in parentheses*), distances, and reddening for each cluster were taken from Harris (1996).

$(V-K)_0$ color and the calibration from Brodie & Huchra (1990), Fusi Pecci et al. (1996) found [Fe/H] $= -1.14$. Most recently, Meylan et al. (2001) uses WFPC2 observations to estimate [Fe/H] $= -0.95 \pm 0.09$ from the RGB slope in the $(V-I)$ CMD.

Our two metallicity determinations for G1 are different, but not inconsistent. We note that the value from the K-$(J-K)$ RGB slope ([Fe/H] $= -1.22 \pm 0.43$) is based on a very small luminosity range, and has quite large errors. The estimate from the appearance of the M_{K_0}-$(V-K)_0$ CMD ([Fe/H] ~ -0.9) is less quantitative, but more robust. The existence of LPVs also points toward the higher [Fe/H] value, since LPVs only occur in clusters with [Fe/H] > -1, at least in our Galaxy (Frogel & Whitelock 1998; Frogel & Elias 1988).

There have been suggestions that the stars in G1 may have a range in metallicity (Jablonka et al. 1999), possibly due to self-enrichment. If this is so, we should be able to detect a spread in color in our near-IR CMDs. However, we find no evidence for such a metallicity spread ($\sigma_{[Fe/H]} < 0.2$) based on the dispersions in the $(J-H)$ color in the range $-3 > M_H > -6$ ($\sigma_{(J-H)} = 0.06$) and the $(J-K)$ color in the range $-4.5 > M_K > -6.5$ ($\sigma_{(J-K)} = 0.04$). Both are very close to the spread expected solely from measurement errors, as predicted by the artificial cluster A1, and by the ALLFRAME photometric uncertainties. We caution though that this Gaussian fit is to the distributions of only 92 and 24 stars in the $(J-H)$ and $(J-K)$ CMDs, and thus it could be adversely affected by small number statistics.

4.3. *G280*

The G280 M_K-$(J-K)$ CMDs are shown in Figure 7. The left panel shows all the data inside a radius of 5″, the radius chosen to define the cluster. Objects inside the threshold-blending limit ($\mu_K < 16$, $r < 2\farcs2$) are plotted with open circles, and objects inside the critical-blending limit ($\mu_K < 14$, $r < 1\farcs0$) are plotted with half-size dots. The center panel shows all objects measured outside the 5″ cluster radius. These stars are expected to be mostly noncluster, or "field," stars. The right panel shows the result of statistically subtracting the field star component from the cluster. We have also omitted objects inside the threshold-blending radius which are most likely to be affected by blending. Thus the right panel only includes objects in the annulus between the threshold-blending radius (2\farcs2) and the cluster radius (5″).

We apply a linear least-squares fit to the cluster stars brighter than $M_K = -3.7$ and $M_J = -2$, ignoring 3 σ outliers. The best-fit equation is displayed at the top of the right panel. Using this slope (-0.136 ± 0.011) and the GB slope-[Fe/H] relationship of Kuchinski & Frogel (1995) we estimate the blending-uncorrected metallicity of the G280 cluster as $+0.26 \pm 0.36$.

Again, as mentioned in § 3.1, the measured slope and thus the calculated metallicity will be affected by blending. As in the case of G1, there are so few stars on the upper GB, that splitting it up into annuli significantly degrades the accuracy of the slope determination. We thus determine the blending correction using the number-weighted average surface brightness of $\mu_K = 16.9$ for the G280 cluster. This indicates a metallicity correction of -0.42 ± 0.09 dex is required to remove the effects of blending. Applying this correction gives a final metallicity of -0.15 ± 0.37 for the G280 cluster.

Previous metallicity measurements for G280 are listed in Table 5, and the techniques were briefly discussed in § 4.2. These measurements cover a fairly large range, but our value is consistent with most.

We also looked for a possible intrinsic color spread, and hence a metallicity spread in G280. Such a metallicity spread would not be too surprising, since G280 is also a very massive cluster, with a velocity dispersion which is actually higher than that of G1 (Djorgovski et al. 1997). However, the dispersion in the measured colors is small, $\sigma_{(J-H)} = 0.07$ $(-3 > M_H > -6)$, $\sigma_{(J-K)} = 0.08$ $(-4.5 > M_K > -6.5)$, only slightly larger than the spread expected solely from measurement errors. Thus we conclude that G280 could have a small metallicity spread of $\sigma_{[Fe/H]} \sim 0.2$. However, as in the G1 cluster, the Gaussian fits are to rather small numbers of stars; only 94 and 51 in the appropriate magnitude ranges of the $(J-H)$ and $(J-K)$ CMDs.

Figure 8 shows the linear fits to the G1 and G280 giant branches before and after the blending correction. Also shown are two Galactic globular clusters with similar metallicities. This figure gives an idea of the relative positions of the G1 and G280 CMDs, as well as the magnitude and direction of the blending corrections applied to the GB slopes.

The luminosity functions of the G1 (*short-dashed*) and G280 (*long-dashed*) clusters are shown in Figure 9 and listed in Table 6. These LFs only include stars measured outside the threshold surface brightness radius. In addition, G1 only includes objects above the high background region of the K-band images ($Y > 25$ pixels), and G280 only includes objects within 5″ of the cluster center. Both LFs appear to

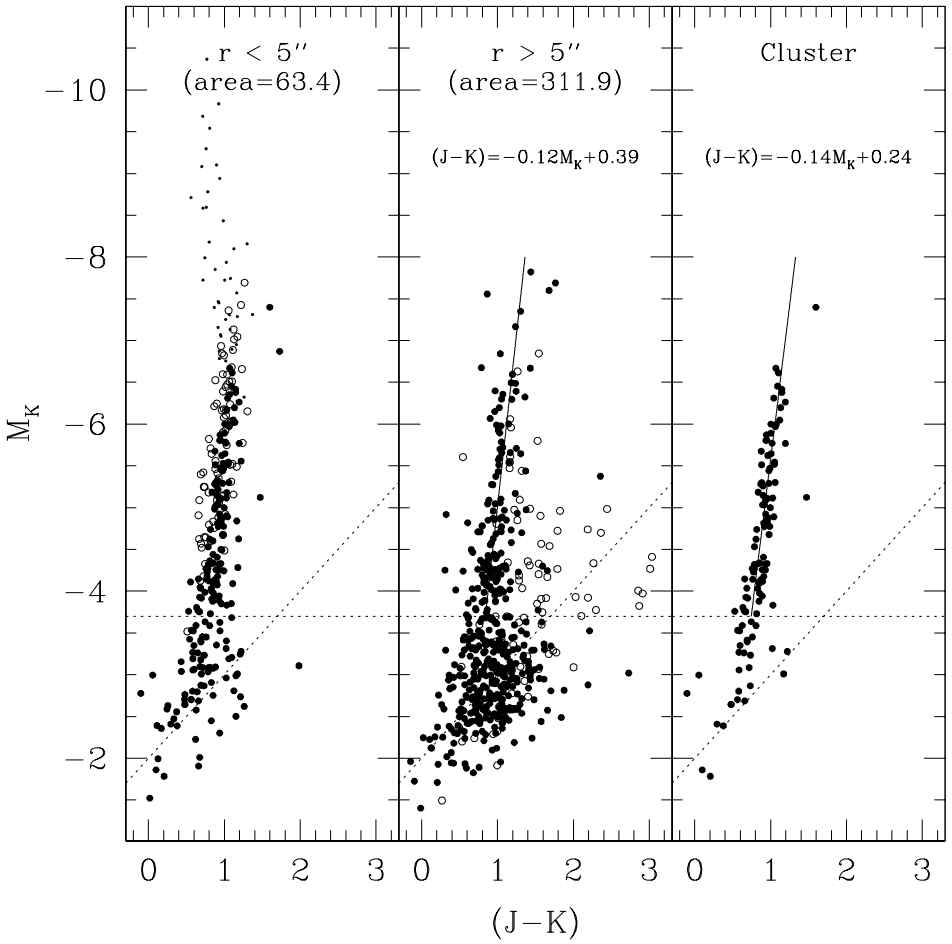


FIG. 7.—*Left*: All 322 objects measured within 5″ of the G280 cluster center. Open circles indicate objects within the threshold-blending limit ($\mu_K < 16, r < 2\farcs2$), and half-size dots are for objects inside the critical-blending radius ($\mu_K < 14$, $r < 1\farcs0$). *Center*: All 536 objects farther than 5″ from the cluster. Open circles represent objects measured in the high-noise region in the bottom 25 pixels of the *K*-band image and are excluded from the GB fit. *Right*: Remaining 115 objects between $2\farcs2 < r < 5\farcs0$ after statistical field subtraction and the linear fit to the GB. The dashed lines at $M_K = -3.7$ and $M_J = -2$ indicate the 50% completeness limits determined from the traditional completeness tests, and all fits disregard data fainter than these limits.

have a sharp cutoff at $M_K \sim -6.5$, which is consistent with what is observed in Galactic globulars (Ferraro et al. 2000; Frogel et al. 1983). The faint end of G280 drops off more quickly than that of G1 since it is closer to the nucleus of M31, and the background is higher, making it more difficult to detect fainter stars. We also show the Galactic bulge LF measured by Frogel & Whitford (1987) in Baade's Window (*solid line*) which has a sharp cutoff at $M_K \sim -7.5$.

TABLE 6

LUMINOSITY FUNCTIONS

	CLUSTERS		FIELDS			
M_K	G1	G280	G170	G174	G177	G280
−8.25.....	0	0	1	5	6	0
−7.75.....	1	0	11	19	58	4
−7.25.....	0	1	24	65	125	2
−6.75.....	0	2	88	237	361	4
−6.25.....	4	7	128	356	533	12
−5.75.....	9	16	213	422	545	15
−5.25.....	6	15	197	445	561	12
−4.75.....	14	13	229	359	322	26
−4.25.....	17	20	229	203	150	57
−3.75.....	25	17	199	109	72	46
−3.25.....	26	12	105	52	26	96
−2.75.....	46	8	49	14	6	112
−2.25.....	34	2	13	4	0	49
−1.75.....	6	2	4	0	1	8
−1.25.....	2	0	0	0	0	0

4.4. *Central Clusters*

The three central clusters (G170, G174, and G177) are so compact that we were unable to extract any photometry of the cluster stars themselves. The star counts indicate that the clusters were detected, but the detections occur in the regime where the effects of blending are considerable. Thus for these three clusters we present only the calibrated field CMDs in § 4.5.1 and field LFs in § 4.5.2.

4.5. *Surrounding Fields*

4.5.1. *G170, G174, and G177*

The CMDs of the fields around the central three clusters are shown in Figure 10. We use the same blending criteria as the other clusters, developed in Paper I. Objects inside the critical-blending radius ($\mu_K < 14$) are plotted with half-size dots, and should be ignored. (see Table 3 for the blend radius of each cluster). These are the brightest and bluest stars on the upper RGB of each field. Objects located inside the threshold-blending radius ($\mu_K < 16$) or in the high back-

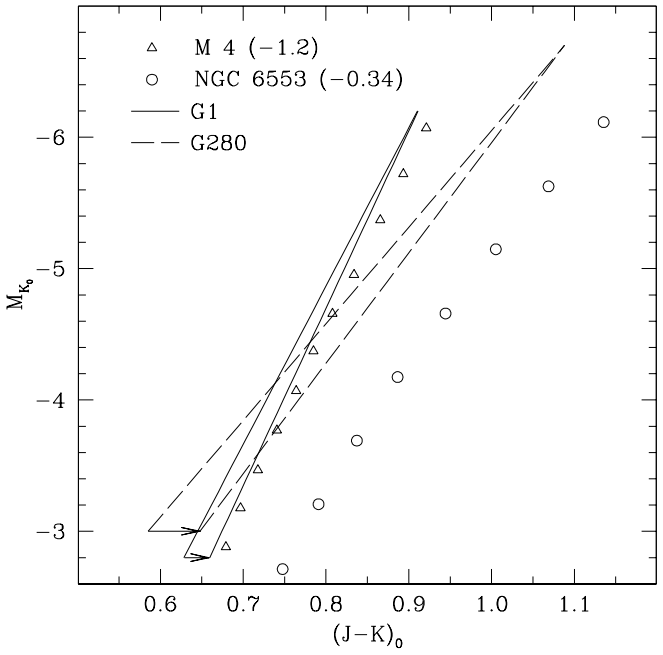


FIG. 8.—Linear fits to the G1 and G280 giant branches. The arrows show the shifts estimated for the blending corrections. For comparison, we also show the GB fits and metallicities of the Galactic globular clusters M4 ([Fe/H] = −1.2) and NGC6553 ([Fe/H] = −0.34). Since we estimate metallicities for the M31 clusters using the slope of the RGB, a quantity which is reddening independent, the absolute color is unimportant. In this plot G1 and G280 have been corrected for distance and reddening with $(m-M)_0 = 24.4$, $A_K = 0.03$, and $E(J-K) = 0.06$. The Galactic clusters are from Ferraro et al. (2000), using distances and reddenings from Harris (1996). For M4: $(m-M)_0 = 11.71$, $A_K = 0.11$, and $E(J-K) = 0.19$; and for NGC6553: $(m-M)_0 = 13.74$, $A_K = 0.23$, and $E(J-K) = 0.39$. Note that we have extended the RGB of M4 by ∼1 mag to match the level of the RGB tip observed by Frogel et al. (1983).

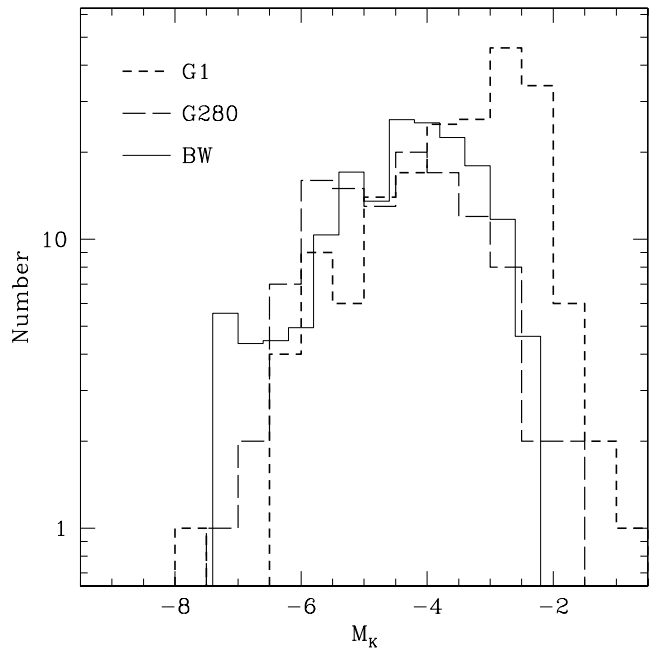


FIG. 9.—G1 (*short dash*) and G280 (*long dash*) cluster luminosity functions. Also shown is the scaled Baade's Window LF (*solid line*) from Frogel & Whitford (1987).

ground region in the bottom 25 pixels of the K-band images are plotted with open circles, and should be viewed with suspicion. We provide a linear fit to the GB measured in the G170 field, but do not attempt to estimate a metallicity, as the effects of blending are greater than we currently feel comfortable trying to correct.

As is evident from the radial surface brightness plots in Figure 4, the stellar density of these central fields is exceedingly high. G174 is the closest to the the nucleus of M31, and G177 is only slightly farther away but lies along M31's major axis. The surface brightness of these two fields never drops below the threshold blending limit. We are therefore skeptical of this photometry, and do not provide GB fits. The artificial cluster A177 (the analog of G177), revealed brightening even in the field of up to 0.6 mag at K due to blending.

4.5.2. *Field Luminosity Functions*

Figure 11 shows the scaled luminosity functions for the fields surrounding the observed clusters. The unscaled LFs are listed in Table 6. We do not give the G1 field as it is assumed that almost all of the stars are cluster members since only two were found in the nearby control field. All fields exclude objects measured in the noisy lower 25 pixels of the K-band images. The G280 field includes all stars measured farther than 5″ from the cluster center. For G170 we only count stars measured outside the threshold blending radius, while for G174 and G177 we take everything outside the critical-blending radius (Table 3), since the entire field is above the threshold surface brightness.

All the field LFs look approximately the same, allowing for differences in the faint end due to varying levels of incompleteness. They all have an upper limit of $M_K \sim -8$, similar to what has been measured in the Galactic bulge where Frogel & Whitford (1987) observed a sharp break at $M_K \sim -7.4$ and stars trailing off to $M_K \sim -8.5$. These observations imply that the bulge of M31 has a stellar population not significantly younger than that in Baade's Window, contrary to some previous observations. We will address this issue in more detail when we present our NICMOS data targeted at M31's bulge

4.5.3. *The G280 Field*

Of all the field observations, the G280 field is the least crowded, and the only one where we feel comfortable performing a detailed giant branch analysis. The field CMD is shown in the center panel of Figure 7. The linear fit to the field GB, rejecting points fainter than $M_K = -3.7$ or $M_J = -2$, objects measured in the high-noise region in the bottom 25 pixels of the K-band frame, as well as $>3\ \sigma$ deviants, is shown at the top of the panel. The measured slope of the GB is -0.122 ± 0.014, which yields a metallicity of -0.07 ± 0.42 from the relation of Kuchinski & Frogel (1995). The average surface brightness of the field is $\mu_K \sim 18.3$, which requires a metallicity correction of -0.23 ± 0.09 dex to compensate for the effects of blending (see § 3.1). Thus our final estimate of the metallicity of the G280 field is -0.30 ± 0.43.

We measure a large spread in color in this field. The dispersion in the $(J-H)$ color is $\sigma_{(J-H)} \sim 0.10$, and the dispersion in the $(J-K)$ color is $\sigma_{(J-K)} \sim 0.11$, both of which are significantly larger than the spread measured in the G1 or G280 clusters. This spread in color is most likely due to a true spread in metallicity, and not to differential reddening

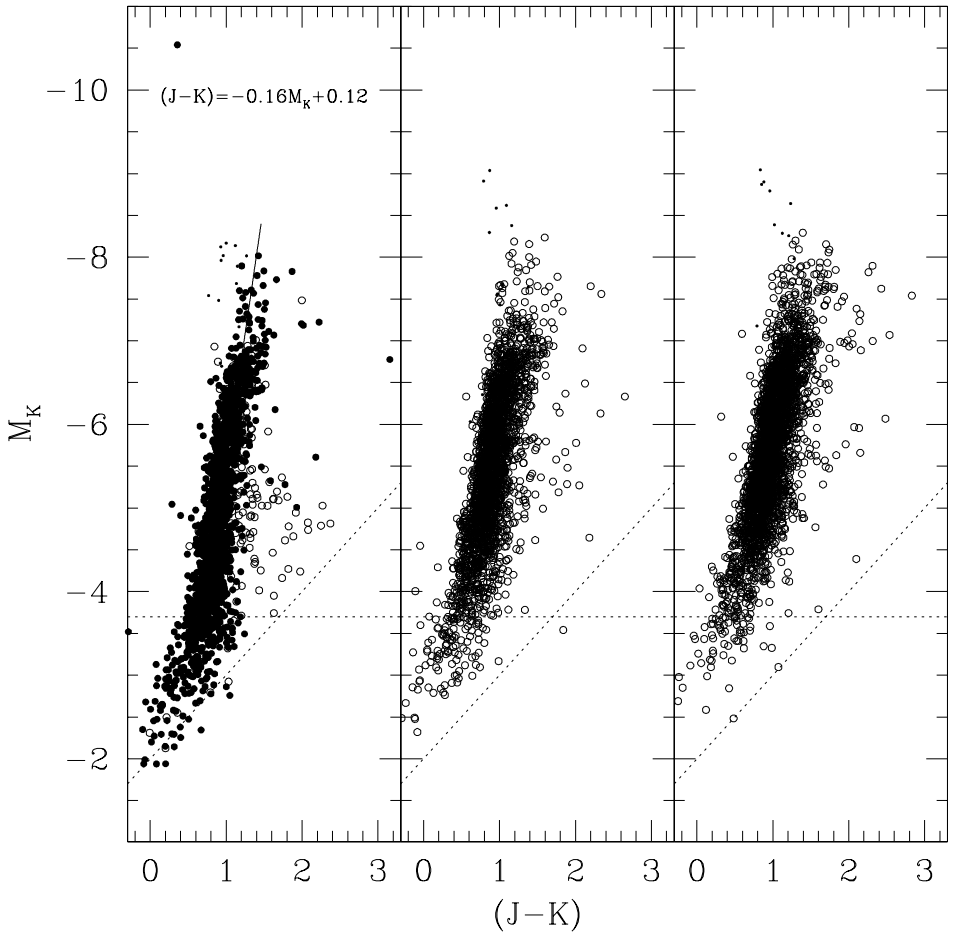


FIG. 10.—CMDs of the fields around G170 (*left*), G174 (*center*), and G177 (*right*). Full size points indicate measurements made in low surface brightness regions. Open circles are for objects measured where $\mu_K < 16$ or in the high background region in the lower 25 pixels of the K-band images. Half-size points are for objects measured where $\mu_K < 14$. We provide a linear fit to the GB of the G170 field, where the crowding is not too severe. This fit ignores points inside the critical-blending radius (*half-size dots*), points inside the threshold-blending radius or in the lower 25 pixels of the K-band image (*open circles*), and objects fainter than $M_K = -3.7$ or $M_J = -2$.

as we shall later show. Such a metallicity spread is not unexpected, since this field samples both the disk and bulge populations.

We use two methods to estimate the spread in metallicity in this field. Frogel, Cohen, & Persson (1983) have empirically determined a relationship between the GB $(J-K)$ color at $M_K = -5.5$ and the cluster metallicity using 12 Galactic globulars with [Fe/H] < -0.8. This relation has been recently revised by Ferraro et al. (2000) using 10 GGCs with more accurate distances: [Fe/H] $= 4.76 \times (J-K)_0(\mathrm{GB})_{-5.5} - 5.38$. The measured spread in $(J-K)$ for the M31-G280 field is $\sigma_{(J-K)} \sim 0.11$ in the range $-4.5 > M_K > -6.5$. We estimate the $(J-K)$ spread due to measurement errors is $\sigma_{(J-K)} \sim 0.06$. Thus the intrinsic spread in color is $\sigma_{(J-K)} \sim 0.09$. Using the Ferraro et al. (2000) relation, this leads to a spread in metallicity of $\sigma_{[\mathrm{Fe/H}]} \sim 0.4$,

Another method is to use the $(J-H)$ color, valuable since our J and H band data are the deepest of our observations. We have used the evolutionary tracks of Girardi et al. (2000) to derive a relation between the GB $(J-H)$ color at $M_H = -4$ and the cluster metallicity. We find that: [Fe/H] $= 4.76 \times (J-H)_0(\mathrm{GB})_{-4.0} - 4.27$. In the G280 field the measured spread in $(J-H)$ is $\sigma_{(J-H)} \sim 0.10$ in the range $-3.0 > M_H > -6.0$. We estimate the spread in $(J-H)$ due to measurement errors is $\sigma_{(J-H)} \sim 0.06$ (also the spread measured in G1). Thus the intrinsic spread in $(J-H)$ color is $\sigma_{(J-H)} \sim 0.08$. Using our relation derived from the evolutionary tracks, this corresponds to a spread in metallicity of $\sigma_{[\mathrm{Fe/H}]} \sim 0.4$, identical to the previous determination.

We thus estimate that the true spread in metallicity for the G280 field is $\sigma_{[\mathrm{Fe/H}]} \sim 0.4$. Note that no correction for blending is required, since our analysis shows no significant effects of blending on the GB width until brighter than $\mu_K \sim 16$ mag arcsec^{-2}.

Since the depth of this field and hence the amount of reddening through the disk of M31 is unknown, we must consider the possibility that some of the observed color spread may be due to differential reddening. G280 has $E(B-V) = 0.10$ (Frogel et al. 1980b), but there are several nearby clusters which, according to the reddening distribution map of Barmby et al. (2000), have reddenings of $0.10 < E(B-V) < 0.20$. If we assume the extreme case, that the reddening in the G280 field may be variable by as much as ± 0.10 in $E(B-V)$, then the infrared reddening $E(J-K)$ would be variable by ± 0.05. However this is small compared to the estimated intrinsic dispersion of $\sigma_{(J-K)} \sim 0.09$.

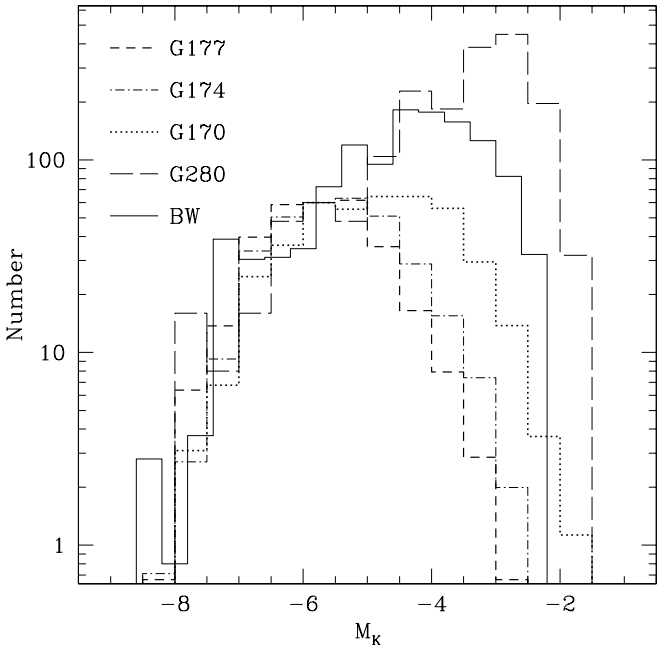


FIG. 11.—Normalized luminosity functions for the fields around each cluster and the Baade's Window LF from Frogel & Whitford (1987). The similarity of these LFs to the BW LF, which exhibits an order of magnitude drop at $M_K \sim -7.4$, indicates that there is no significant population of bright young stars in the bulge of M31.

Even if variable reddening in the field contributed a color spread of 0.05, the implied metallicity spread would only be reduced by 16% (from 0.43 to 0.36 dex).

5. CONCLUSIONS

We first present images (Figs. 1 and 2) and surface brightness profiles (Fig. 4) of all clusters, and with the blending analysis presented in Paper I, determine radial photometric limits for each cluster. We then give integrated photometry of all clusters except G1, which was not fully on the detector (Table 4).

For the G1 cluster, we present the infrared CMD (Fig. 5), and estimate the metallicity as [Fe/H] $= -1.22 \pm 0.43$ from the slope of the giant branch. Based on the width of the giant branch, which shows no significant spread in color over what is expected from measurement errors alone ($\sigma_{(J-H)} = 0.06$), we conclude that there is no significant metallicity spread in the cluster ($\sigma_{[Fe/H]} < 0.2$). We combine our infrared observations of G1 with two epochs of optical V-band *HST*-WFPC2 data, revealing that several of the brightest stars in the cluster are LPVs. The shape and position of the GB in the M_{K_0}-$(V-K)_0$ CMD (Fig. 6) are similar to that of M107, indicating a metallicity of [Fe/H] $= -0.9 \pm 0.2$. Because of the minimal luminosity range of the IR CMD fit, and the presence of LPVs in G1, we place more weight on the higher metallicity estimate.

For the G280 observations, we divide the frame into cluster and field at a radius of 5″ from the cluster center. We statistically subtract the field population from the cluster, and present both the cluster and field CMDs (Fig. 7). Fitting the giant branch, we find a cluster metallicity of [Fe/H] $= -0.15 \pm 0.37$. We see marginal evidence for a metallicity spread in the cluster based on the width of the GB ($\sigma_{[Fe/H]} \lesssim 0.2$).

Fitting the GB of the G280 field, we find a metallicity of -0.3 ± 0.4. We also estimate a spread in metallicity of $\sigma_{[Fe/H]} \sim 0.4$ dex from the width of the GB. This is not surprising, since this field has contributions from both the disk (85%) and bulge (15%).

The three central clusters, G170, G174, and G177, are all too compact to extract cluster star photometry. We thus present the field CMDs without trying to separate the cluster and field star contributions (Fig. 10). The surface brightness of the G170 field is within acceptable limits, so we perform a linear fit to the GB, but we do not try to estimate the metallicity, as the blending correction would be uncomfortably large. The G174 and G177 fields, on the other hand, are both above the threshold-blending surface brightness limit. This implies that measurements of all but the brightest stars in these fields are potentially affected by blending, so we refrain from fitting their GBs.

Finally we present the cluster (G1 and G280) LFs in Figure 9 and the field LFs in Figure 11. The luminosity functions of G1 and G280 both have a sharp bright-end cutoff at $M_K \sim -6.5$, consistent with observations of Galactic globulars. The fields surrounding the clusters have LFs which are indistinguishable from that measured in the Galactic bulge, with a break at $M_K \sim -7.5$. Thus, at least in the fields observed, there is no significant population of young luminous stars in the bulge of M31.

Support for this work was provided by NASA through grant GO-7826 from the Space Telescope Science Institute. R. M. R. acknowledges additional support from NASA contract NAG 5-9431, awarded in connection with the NGST ad hoc science working group. Thanks to Peter Stetson for supplying, and helping us with his photometry package, ALLFRAME. Valuable comments from Judy Cohen, Darren DePoy, Paul Martini, and Marcia Rieke were greatly appreciated. We would also like to thank the anonymous referee who provided an extremely thorough and detailed report, which significantly improved this paper.

REFERENCES

Ajhar, E. A., Grillmair, C. J., Lauer, T. R., Baum, W. A., Faber, S. M., Holtzman, J. A., Lynds, C. R., & O'Neil, E. J., Jr. 1996, AJ, 111, 1110
Barbuy, B., Renzini, A., Ortolani, S., Bica, E., & Guarnieri, M. D. 1999, A&A, 341, 539
Barmby, P., Huchra, J. P., Brodie, J. P., Forbes, D. A., Schroder, L. L., & Grillmair, C. J. 2000, AJ, 119, 727
Battistini, P., Bonoli, F., Braccesi, A., Federici, L., Fusi Pecci, F., Marano, B., & Borngen, F. 1987, A&AS, 67, 447
Bica, E., Jablonka, P., Santos, J. F. C., Jr., Alloin, D., & Dottori, H. 1992, A&A, 260, 109
Bònoli, F., Delpino, F., Federici, L., & Fusi Pecci, F. 1987, A&A, 185, 25
Brodie, J. P., & Huchra, J. P. 1990, ApJ, 362, 503
Burstein, D., Faber, S. M., Gaskell, C. M., & Krumm, N. 1984, ApJ, 287, 586
Cohen, J. G., Gratton, R. G., Behr, B. B., & Carretta, E. 1999, ApJ, 523, 739
Cohen, J. G., & Matthews, K. 1994, AJ, 108, 128
Djorgovski, S. G., Gal, R. R., McCarthy, J. K., Cohen, J. G., De Carvalho, R. R., Meylan, G., Bendinelli, O., & Parmeggiani, G. 1997, ApJ, 474, L19
Elson, R. A. W., & Walterbos, R. A. M. 1988, ApJ, 333, 594
Ferraro, F. R., Montegriffo, P., Origilia, L., & Fusi Pecci, F. 2000, AJ, 119, 1282
Frogel, J. A., Cohen, J. G., & Persson, S. E. 1983, ApJ, 275, 773
Frogel, J. A., & Elias, J. H. 1988, ApJ, 324, 823
———. 1980b, ApJ, 240, 785
———. 1980c, in Globular Clusters, ed. D. Hanes & B. Madore (Cambridge: Cambridge Univ. Press), 159
———. 1981, ApJ, 246, 842
———. 1983, ApJS, 53, 713
Frogel, J. A., & Whitelock, P. A. 1998, AJ, 116, 754
Frogel, J. A., & Whitford, A. E. 1987, ApJ, 320, 199

Fusi Pecci, F., Buonanno, R., Cacciari, C., Corsi, C. E., Djorgovski, G., Federici, L., Ferraro, F. R., Parmeggiani, G., & Rich, R. M. 1996, AJ, 112, 1461
Girardi, L., Bressan, A., Bertelli, G., & Chiosi, C. 2000, A&AS, 141, 371
Guarnieri, M. D., Ortolani, S., Montegriffo, P., Renzini, A., Barbuy, B., Bica, E., & Moneti, A. 1998, A&A, 331, 70
Harris, H. C., & Canterna, R. 1977, AJ, 82, 798
Harris, W. E. 1996, AJ, 112, 1487
Heasley, J. N., Christian, C. A., Friel, E. D., & Janes, K. A. 1988, AJ, 96, 1312
Huchra, J. P., Brodie, J. P., & Kent, S. M. 1991, ApJ, 370, 495
Jablonka, P. 1997, in Galaxy Scaling Relations: Origins, Evolution, and Applications, ed. L. da Costa & A. Renzini (New York: Springer), 140
Jablonka, P., Alloin, D., & Bica, E. 1992, A&A, 260, 97
Jablonka, P., Bridges, T. J., Sarajedini, A., Meylan, G., Maeder, A., & Meynet, G. 1999, ApJ, 518, 627
Jablonka, P., Courbin, F., Meylan, G., Sarajedini, A., Bridges, T. J., & Magain, P. 2000, A&A, 359, 131
Kuchinski, L. E., & Frogel, J. A. 1995, AJ, 110, 2844
Kuchinski, L. E., Frogel, J. A., Terndrup, D. M., & Persson, S. E. 1995, AJ, 109, 1131
MacKenty J. W., et al. 1997, NICMOS Instrument Handbook, Version 2.0 (Baltimore: STScI)
Meylan, G., Sarajedini, A., Jablonka, P., Djorgovski, S. G., Bridges, T., & Rich, R. M. 2001, in preparation
Renzini, A. 1986, in Stellar Populations, ed. C. A. Norman, A. Renzini, & M. Tosi (Cambridge: Cambridge Univ. Press), 213
Rich, R. M., Mighell, K. J., Freedman, W. L., & Neill, J. D. 1996, AJ, 111, 768
Sargent, W. L. W., Kowal, C. T., Hartwick, F. D. A., & van den Bergh, S. 1977, AJ, 82, 947
Seitzer, P., Banas, K. R., & Armandroff, T. 1996, BAAS, 189, 7117
Stephens, A. W., Frogel, J. A., Freedman, W., Gallart, C., Jablonka, P., Ortolani, S., Renzini, A., Rich, R. M., & Davies, R. 2001, AJ, 121, 2584 (Paper I)
Stephens, A. W., Frogel, J. A., Ortolani, S., Davies, R., Jablonka, P., Renzini, A., & Rich, R. M. 2000, AJ, 119, 419
Stetson, P. B. 1990, PASP, 102, 932
———. 1994, PASP, 106, 250
Zinn, R. J., & West, M. J. 1984, ApJS, 55, 45